Journal of Applied Physics

Bulk single crystals and physical properties of β-$(Al_xGa_{1-x})_2O_3$ (x = 0–0.35) grown by the Czochralski method

Cite as: J. Appl. Phys. **133**, 035702 (2023); https://doi.org/10.1063/5.0131285
Submitted: 19 October 2022 • Accepted: 28 December 2022 • Published Online: 18 January 2023

Zbigniew Galazka, Andreas Fiedler, Andreas Popp, et al.

AIP Publishing

Journal of Applied Physics ARTICLE scitation.org/journal/jap

Bulk single crystals and physical properties of β-$(Al_xGa_{1-x})_2O_3$ (x = 0–0.35) grown by the Czochralski method

Cite as: J. Appl. Phys. **133**, 035702 (2023); doi: 10.1063/5.0131285
Submitted: 19 October 2022 · Accepted: 28 December 2022 ·
Published Online: 18 January 2023

Zbigniew Galazka,[1,a)] Andreas Fiedler,[1] Andreas Popp,[1] Steffen Ganschow,[1] Albert Kwasniewski,[1] Palvan Seyidov,[1] Mike Pietsch,[1] Andrea Dittmar,[1] Saud Bin Anooz,[1] Klaus Irmscher,[1] Manuela Suendermann,[1] Detlef Klimm,[1] Ta-Shun Chou,[1] Jana Rehm,[1] Thomas Schroeder,[1,2] and Matthias Bickermann[1,3]

AFFILIATIONS

[1]Leibniz-Institut für Kristallzüchtung, Max-Born-Str. 2, 12489 Berlin, Germany
[2]Humboldt-Universität zu Berlin, Institut für Physik, Newtonstr. 15, 12489 Berlin, Germany
[3]Technische Universität Berlin, Institut für Chemie, Straße des 17. Juni 115, 10623 Berlin, Germany

[a)]**Author to whom correspondence should be addressed:** zbigniew.galazka@ikz-berlin.de

ABSTRACT

We have systematically studied the growth, by the Czochralski method, and basic physical properties of a 2 cm and 2 in. diameter bulk β-$(Al_xGa_{1-x})_2O_3$ single crystal with [Al] = 0–35 mol. % in the melt in 5 mol. % steps. The segregation coefficient of Al in the Ga_2O_3 melt of 1.1–1.2 results in a higher Al content in the crystals than in the melt. The crystals were also co-doped with Si or Mg. [Al] = 30 mol. % in the melt (33–36 mol. % in the crystals) seems to be a limit for obtaining bulk single crystals of high structural quality suitable for homoepitaxy. The crystals were either semiconducting (no intentional co-dopants with [Al] = 0–30 mol. % and Si-doped with [Al] = 15–20 mol. %), degenerately semiconducting (Si-doped with [Al] ≤ 15 mol. %), or semi-insulating ([Al] ≥ 25 mol. % and/or Mg-doped). The full width at half maximum of the rocking curve was 30–50 arcsec. The crystals showed a linear but anisotropic decrease in all lattice constants and a linear increase in the optical bandgap (5.6 eV for [Al] = 30 mol. %). The room temperature electron mobility at similar free electron concentrations gradually decreases with [Al], presumably due to enhanced scattering at phonons as the result of a larger lattice distortion. In Si co-doped crystals, the scattering is enhanced by ionized impurities. Measured electron mobilities and bandgaps enabled to estimate the Baliga figure of merit for electronic devices.

I. INTRODUCTION

In the last decade, β-Ga_2O_3 experiences enormous development in bulk crystal growth technology, epitaxial film growth, device fabrication, and exploring underlying physics of that compound. This is the result of a large bandgap of 4.85 eV[1], a wide doping range, high carrier mobility, and high theoretical breakdown field of 8 MV/cm.[2] Furthermore, the availability of large single crystals and different epitaxial techniques allows us to fabricate devices for a diversity of applications. They include high power electronics, UV optoelectronics, radiation detectors, and high temperature gas sensing. In addition to the rich literature, the above-mentioned areas are discussed in a number of review articles and books.[3–17] A particular attention is paid to high power switching devices that are economical and environmentally friendly. To enhance the capability of switching high voltages, β-Ga_2O_3 is being doped with aluminum (Al) that increases the bandgap and, thus, the breakdown field.

Doping of β-Ga_2O_3 with Al has been discussed theoretically and conducted experimentally for both thin films and bulk crystals. Peelaers *et al.*[18] and Varley *et al.*[19,20] theoretically explored structural, electronic, and optical properties of β-$(Al_xGa_{1-x})_2O_3$ with the following conclusions: (i) the Al content can be as high as about

50%, (ii) the lattice constants decrease, while the bandgap increases with Al concentration, and (iii) Si is an effective shallow donor dopant over the whole Al doping range. As β-$(Al_xGa_{1-x})_2O_3$ films are grown heteroepitaxially so far (due to the lack of such substrates), Mu *et al.*[21] discuss cracking and limits of the films when grown on β-Ga_2O_3. Thin films of β-$(Al_xGa_{1-x})_2O_3$ were grown heteroepitaxially only by Kaun *et al.*[22] using MBE, and Bhuiyan *et al.*[23–26] and Alema *et al.*[27] using MOCVD, while Johnson *et al.*[28] discuss defect formation both theoretically and experimentally in such films. Kaun *et al.*[22] pointed to 18 mol. % of [Al] as a limit in thin films, while Bhuiyan *et al.*[23,29] reported phase segregation in thin films at [Al] > 27 mol. %. Furthermore, Bhuiyan *et al.*[25] discussed the superlattices of the (100) β-Ga_2O_3–β-$(Al_xGa_{1-x})_2O_3$ system with a film thickness of <90 nm. The authors demonstrated Al incorporation up to 52 mol. % in the superlattices, but the structural quality of the films significantly deteriorated with [Al]. Additionally, growing β-Ga_2O_3 on (100)-oriented wafers without a dedicated miscut by 2–6° toward [00$\bar{1}$] always results in a very high density of twins, with very poor or even not measurable electrical properties due to dangling bonds acting as compensating acceptors.[30–32]

Bulk β-$(Al_xGa_{1-x})_2O_3$ single crystals with x = 0.05, including 2–in. diameter, and co-doped with Si, and Si + Ce were grown by Galazka *et al.*[33–36] by the Czochralski method. Al-doped crystals were semiconducting, but with a bit lower electron mobility as compared to pure β-Ga_2O_3. The Czochralski method for that compound was also utilized by Bauman *et al.*[37] (x = 0.075) and Jesenovec *et al.*[38] (x = 0.1), wherein obtained crystals were electrically insulating. In the latter case, growth trials with x = 0.33 and 0.5 resulted in polycrystals. Small β-$(Al_xGa_{1-x})_2O_3$ crystals with x = 0.14 were also grown by the OFZ method by Bhaumik *et al.*[39] with no electrical data provided.

The aim of the present work is threefold: (i) to demonstrate the growth of bulk β-$(Al_xGa_{1-x})_2O_3$ single crystals with very high Al concentration (up to 35%) and of high structural quality that are suitable for wafer fabrication and homoepitaxy; (ii) to get different electrical states of such crystals, from semi-insulating, through semiconducting, to degenerately semiconducting; and (iii) to reveal real structural, optical, and electrical properties, including the estimation of the Baliga figure of merit (BFOM), which can only be assessed for electrically conducting crystals.

II. EXPERIMENTAL METHODS

A. Crystal growth

20 and 55 mm diameter β-$(Al_xGa_{1-x})_2O_3$[40] were grown by the Czochralski method utilizing Ir crucibles and inductive heating, as we described in detail in a number of papers.[17,33,34,35,36,41–45] For 20 mm diameter crystals, the growth rate of 1.5 mm/h ([Al] < 10 mol. %) or 1.25 mm/h ([Al] ≥ 10 mol. %), and a rotation rate of 9 rpm were used, while the oxygen concentration in the growth atmosphere was 2 ± 0.5 vol. %. [Al] in the melt was chosen to be between 0 and 30 mol. % in 5 mol. % steps. Other series of crystals with [Al] = 0–35 mol. % in the melt were additionally co-doped with Si = 0.2 or 1 mol. % or with Mg = 0.3 mol. % to enhance electrical conductivity or to compensate it, respectively. For all growth runs, the same batch of starting materials was used (5N Ga_2O_3 and 4.5N Al_2O_3). The heating and cooling times of 10 and 15h, respectively, were the same for all crystals. 55 mm diameter crystals were grown at the growth rates as discussed above and rotation rates of 5–7 rpm, and an oxygen concentration in the growth atmosphere was 10–14 ± 1 vol. %, lower than that for pure β-Ga_2O_3[42] due to better thermal stability. [Al] in the melt ranged between 0 and 20 mol. %, while [Mg] = 0.5 mol. %. Here, the heating and cooling times were 12 and 18 h, respectively, in each case. It should be noted that the equilibrium segregation coefficient for [Al] ≤ 5 mol. % in the Ga_2O_3 melt is about 1.1.[33] Therefore, the Al concentration in the obtained crystals is higher in the crystals than that in the melt (for more details, see Sec. III A). In all cases, the seed composition was the same as that of the melt composition or differed by not more than 5 mol. % of Al (higher or lower). Otherwise, the structural quality of the growing crystal would be significantly deteriorated.

B. Crystal structure

The real structure of the crystals was evaluated by using two techniques: (i) x-ray powder diffraction (XRD) of a powdered crystal using a diffractometer system XRD 3003 TT (GE Inspection Technologies) utilizing a Bragg–Brentano design with a Cu-K-alpha1/2 radiation source. The same equipment was applied for lattice constant determination using Si powder as an external standard; (ii) rocking curves were measured using a high resolution x-ray diffractometer system HR XRD Master (Seifert) equipped with a Bartels monochromator Ge(220) and by choosing an aperture of 2 mm.

C. Electrical properties

The electrical conductivity and Hall effect of the crystals were measured in van der Pauw configuration at room temperature (RT) using a Hall measurement system HMS 7504 (Lake Shore). The contacts were prepared by rubbing a small quantity of the In–Ga eutectic mixture at four points on the rim of as-cleaved wafer-shaped samples of 5 × 5 × 0.5 mm^3 in size. Ohmic behavior of these contacts was accomplished by discharging a capacitor over each two contacts. Electrical setup and sample dimensions limited resistivity measurements to values up to about 10^8 Ω cm. Therefore, samples with higher resistivity could not be measured and are indicated as electrically insulating. Electron concentration and mobility were calculated under the assumption of a unity Hall scattering factor of $r = 1$.

D. Optical absorbance

The spectra were recorded in the transmission mode at room temperature (RT) using a spectrophotometer Lambda 1050 (PerkinElmer) in the wavelength range from 200 to 850 nm. Polarization-dependent transmission was measured using automatically rotatable Glan–Thompson polarizers with a spectral application range of 240–2500 nm. For wavelengths below 240 nm, complete polarization cannot be guaranteed. However, the polarization was sufficient enough to determine the absorption edge. For the measurement of the near-edge absorption spectra, thin cleaved

(100)-oriented samples of 80–200 μm and an aperture of 3 mm diameter were used.

E. Chemical analysis

The dopant concentration (Al and other impurities) was measured by inductively coupled plasma-optical emission spectrometry (ICP-OES), and additionally, secondary ion mass spectroscopy (SIMS) was used to determine the Si content. For ICP-OES, equipment from Thermo Fisher Scientific GmbH (model iCAP 7400 Duo) was used. The spectrometer was calibrated with synthetic solution standards. The samples were prepared by microwave digestion with diluted $HCl + HNO_3$ (220 °C, 20 min). For SIMS measurements, the Cameca IMS 6F model was used with standards prepared by Si ion implantation into β-Ga_2O_3 single crystals.

III. RESULTS AND DISCUSSION

A. Crystal growth

The growth of β-$(Al_xGa_{1-x})_2O_3$ single crystals from the melt can be better understood in connection with the phase diagram shown in Fig. 1(a).[46] At high temperatures, there is no phase transition up to $[Al_2O_3] = 60–70$ mol. %, and the system remains monoclinic. The melting point of the Ga_2O_3–Al_2O_3 system systematically increases with $[Al_2O_3]$, reaching about 1885 °C at $[Al_2O_3] = 30$ mol. %. Indeed, temperature measured during growth experiments, i.e., upon melting, as shown by red dots in Fig. 1(a), is consistent with those in the phase diagram. In this system, the solidus (dashed line) is separated from the liquidus (solid line) with the region in between being in equilibrium between liquid and solid. For example, at $[Al_2O_3] = 30–40$ mol. %, the solidus–liquidus separation is as high as about 50 K. That separation (constitutional supercooling) forces the initial crystallization at much higher [Al] than that in the melt (horizontal red arrow), and next, the crystallization proceeds with a decreasing [Al] (arc red arrow). At low [Al] < 10 mol. %, the difference in the Al content between the first crystallized fraction, CR, and that in the melt is small and results in the effective segregation coefficient just above unity, in line with our previous finding, $k_{eff}(Al) = 1.1$.[33] However, it increases with [Al], leading to a higher effective segregation coefficient $k_{eff}(Al) = 1.2$. This is well shown in Fig. 1(b), which depicts a relation between [Al] in the crystals measured by ICP-OES and initial [Al] in the melt. [Al] in the crystals is higher than that in the melt and also higher at lower CR values. This fits well the phase diagram. For instance, at [Al] = 30% in the melt, the first crystallized fraction (CR = 4%) contains 36 mol. % Al, while the lower part of the crystal (CR = 17%) contains 33 mol. % Al. The same relation is valid for [Al] = 35 mol. %. A value Δ[Al] (difference between the crystal seed and the first crystallized fraction) of below 10 mol. % is still acceptable for obtaining a single crystal, but a higher difference may result in the formation of polycrystalline grains, which often appear at [Al] ≥ 30 mol. %, according to the present study. Growing from a supercooled melt decreases [Al] in the initially crystallized fraction, but highly supercooled melt will also lead to polycrystalline formation. This is due to both fast crystallization, and baroclinic and Marangoni instabilities, which form cooler spots (by 5–10 K) locally on the melt surface, and spontaneous

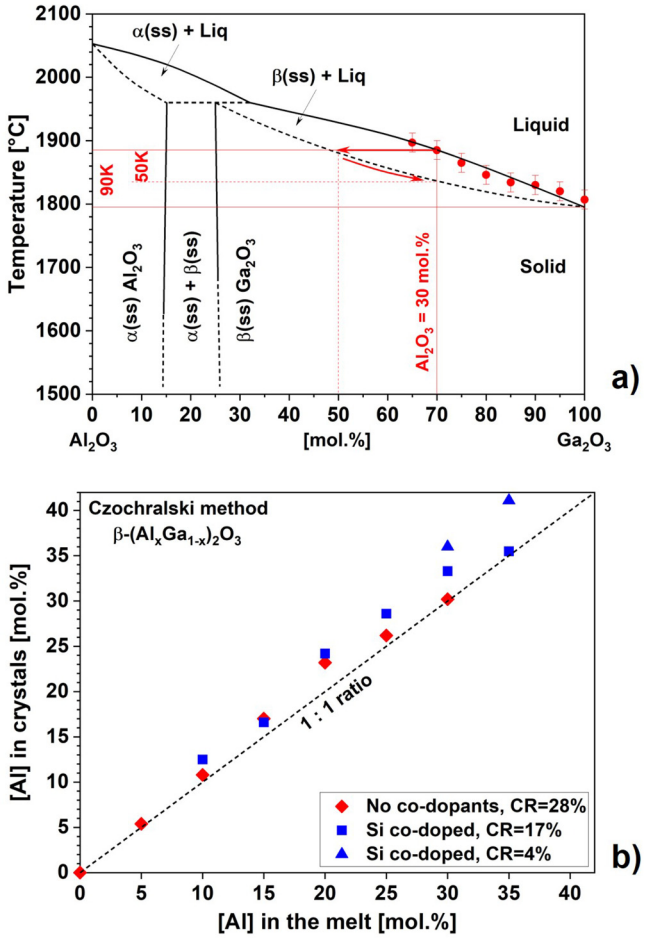

FIG. 1. (a) Phase diagram of the Ga_2O_3–Al_2O_3 system. Reproduced from Ref. 46 with some modifications and additions (in red). Red dots are measured temperature values upon melting of $(Al_xGa_{1-x})_2O_3$ in Czochralski growth experiments, and (b) a relation between [Al] in the melt and in crystals measured by ICP-OES (standard deviation = ±0.15 mol. %). CR is the crystallized fraction, which was a subject of [Al] determination.

parasitic crystallization adjacent to the seed (due to constitutional supercooling). Therefore, the growth of β-$(Al_xGa_{1-x})_2O_3$ single crystals with high [Al] is really challenging due to the above-mentioned thermodynamic issues, including Al segregation, and constitutional supercooling, and rather limited to [Al] = 30 mol. % in the melt.

In the following, [Al] in the discussions and graphs is referred to the initial concentration in the melt (unless otherwise stated), keeping in mind that [Al] in the obtained crystals is higher by 0–6 mol. % depending on the initial [Al] in the melt. So, the real crystal composition can be described as β-$(Al_{x+y}Ga_{1-x-y})_2O_3$, where x is an initial [Al] in the melt, while $y = 0–0.06$ is an additional [Al] in the crystals arising from the effective segregation coefficient that is greater than unity (1.1–1.2) and from the crystallization ratio.

Figure 2(a) shows the photographic images of three series of Czochralski-grown β-$(Al_xGa_{1-x})_2O_3$ single crystals with [Al] = 0–30 mol. % in the melt with no intentional co-doping (first row) and with [Al] = 0–0.35 mol.% and co-doped with Si (second row), as well as with [Al] = 0–25 mol. % and co-doped with Mg (third row). All the crystals with [Al] = 0–25 mol. % were single crystals with no poly-grains, which partly appeared on the crystal surface at [Al] = 30 mol. % for both series of crystals (grains constituting ~10%–20% of the crystal volumes), which extended to almost whole crystal at [Al] = 35 mol. %. All of them crystallized in a monoclinic system according to XRD powder diffraction. β-$(Al_xGa_{1-x})_2O_3$ single crystals with no intentional co-doping are all straight cylinders with almost the same growth interface deflection (Fig. 3) and bluish coloration indicating semiconducting behavior due to the presence of free charge carriers (see Sec. III C). Some of the crystals had one or more twins parallel to (100) and occasionally small cracks parallel to (100) and (001) at the near-surface region. The crystals co-doped with Si are shorter with a cylindrical length of 20–25 mm, beyond which a foot or spiral forms. This is due to free carrier absorption that absorbs heat in the near-infrared

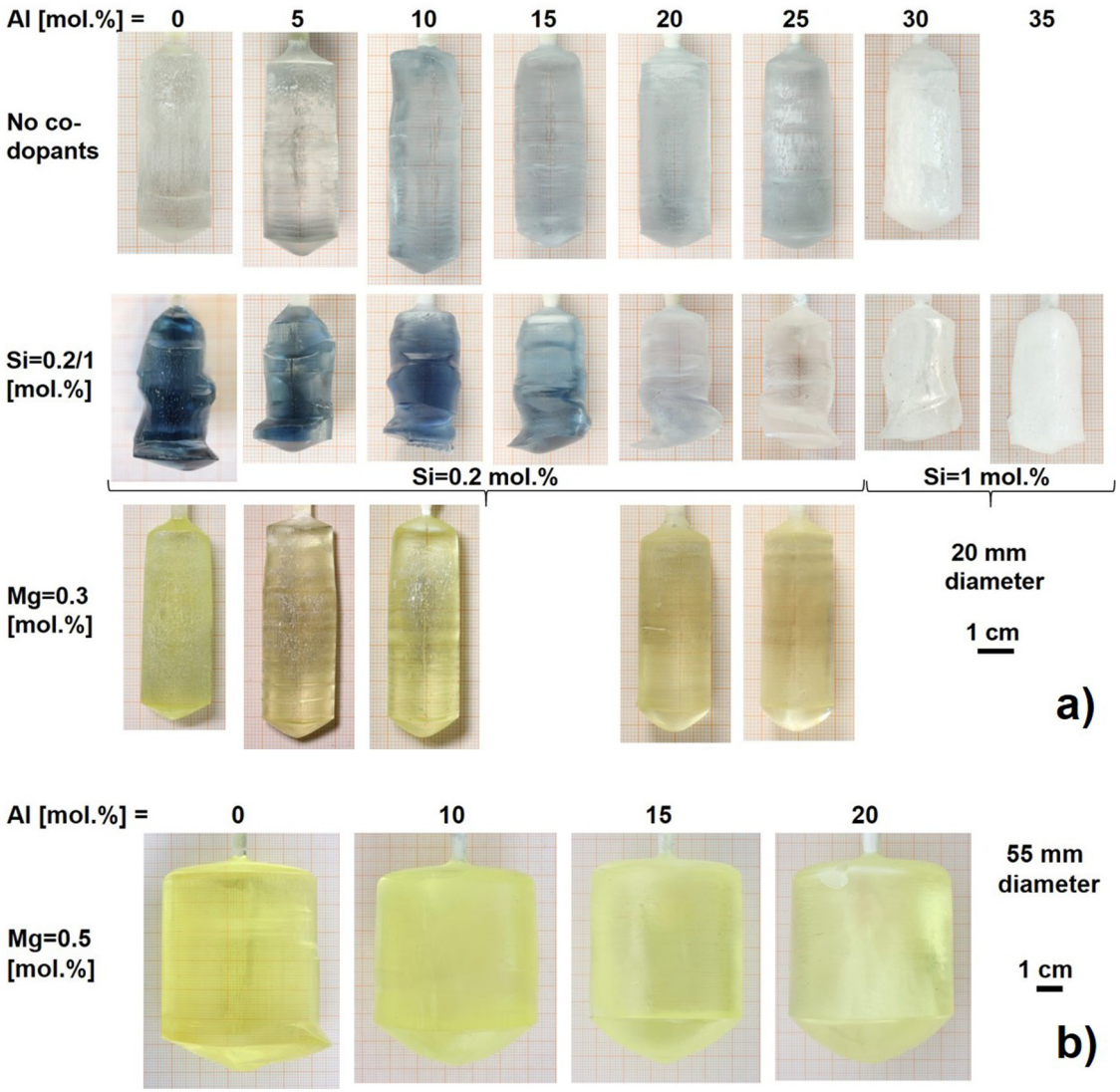

FIG. 2. β-$(Al_xGa_{1-x})_2O_3$ single crystals grown by the Czochralski method: (a) 20 mm diameter with x = 0–0.3 in the melt and no other intentional doping (first row); with x = 0–0.35 and co-doped with Si = 0.2 or 1 mol. % in the melt (second row), and with x = 0–0.25 and co-doped with Mg = 0.3 mol. % in the melt (third row), and (b) 55 mm (2–in.) diameter crystals with x = 0–0.2 and Mg = 0.5 mol. % in the melt.

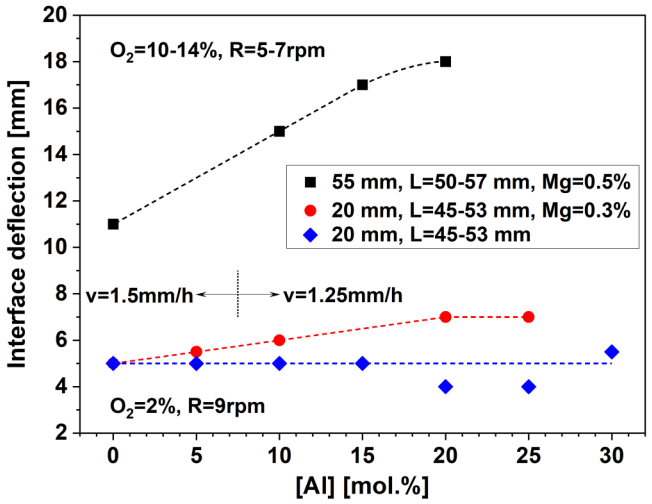

FIG. 3. Interface deflection of β-$(Al_xGa_{1-x})_2O_3$ single crystals (20 and 55 mm in diameter) grown by the Czochralski method vs [Al]. L—cylinder length (excluding shoulder and tail lengths), R—crystal rotation rate, v—crystal growth rate, and O_2—oxygen concentration in the growth atmosphere (vol. %).

spectrum that is accumulated in a growing crystal and causes interface inversion after reaching a certain length. We have discussed this phenomenon in detail in numerous reports.[17,34,35,36,41,43,44] Remarkably, the weakening of the color intensity occurs with increasing [Al], and the color vanishes at high [Al] ≥ 25 mol. % in contrast to crystals doped with Al only, which all show bluish coloration. This clearly indicates a decrease in the free electron concentration (see Sec. III C). However, a tendency of the crystals with [Al] ≥ 25 mol. % co-doped with Si (whether 0.2 or 1 mol. %) to foot or spiral formation, despite an electrically insulating state at RT, clearly indicates high electrical conductivity during growth. We conclude that the Si doping must be responsible for the high electrical conductivity during growth, even though the electrically insulating state at RT is not fully understood, yet (see Sec. III C).

β-$(Al_xGa_{1-x})_2O_3$ single crystals co-doped with Mg are all straight cylinders with slightly increasing interface deflection with [Al] and yellow in color. The increased interface deflection (Fig. 3) points to better transparency in the NIR spectral region with a significantly reduced density of residual free electrons (very high electrical resistivity), which should minimize residual leakage current in electronic devices. Indeed, all the crystals were electrically insulating with no measurable Hall effect.

55 mm (2–in.) diameter β-$(Al_xGa_{1-x})_2O_3$ single crystals co-doped with Mg and about 2–in. long [Fig. 2(b)] are straight cylinders with increasing interface deflection (Fig. 3), and yellow coloration, indicating an electrically insulating state with no measurable Hall effect. They are all single crystals with one or several twins and small cracks observed in some of the crystals. The crystals ensure a large volume for wafer fabrication to be used for homoepitaxial purpose.

B. Crystal structure

Figure 4 depicts the x-ray rocking curves of (100)-oriented samples prepared from 20 mm diameter β-$(Al_xGa_{1-x})_2O_3$ single crystals for [Al] = 0–30 mol. %. The full width at half maximum (FWHM) of the rocking curves of the (400) reflection is typically between 30 and 50 arcsec for [Al] = 0–25 mol. % for both 20 mm and 55 mm diameter crystals. Smooth and narrow rocking curves indicate low-angle grain boundaries in the investigated samples. FWHM values are very similar to each other for [Al] = 0–25 mol. %, but in average, they slightly increase with an Al content as compared to pure β-Ga_2O_3 (typically 18–30 arcsec), which is due to a larger lattice distortion. For [Al] = 30 mol. % ([Al] = 33–36% in the crystal), the rocking curve is much broader with FWHM = 150 arcsec, pointing to a larger density of microscopic structural defects in addition to a larger lattice distortion. Using crystal seeds of a composition having a better match with the first crystallized fraction (i.e., $[Al]_{SEED} > [Al]_{MELT}$) may improve the structural quality of obtained crystals with [Al] ≥ 30 mol. %.

Indeed, all lattice constants in Fig. 5(a) linearly decrease with [Al] in β-$(Al_xGa_{1-x})_2O_3$ crystals with the a-axis having the largest drop (−0.0055 Å/mol. %), followed by the c-axis (−0.0022 Å/mol. %) and b-axis (−0.0017 Å/mol. %). Anisotropic shrinkage of the lattice constants causes an increase (also linear) in angle β between the [100] and [001] crystallographic directions (0.0055°/mol. %).

C. Electrical properties

Czochralski-grown β-$(Al_xGa_{1-x})_2O_3$ single crystals already show semiconducting behavior with no intentional co-doping (i.e., unintentionally doped with free carriers—UID). The free electron concentration, n_e, is confined to a range of $0.4–3 \times 10^{17}$ cm^{-3} for [Al] = 0–25 mol. % as shown in Fig. 6(a) [crystals from the first row

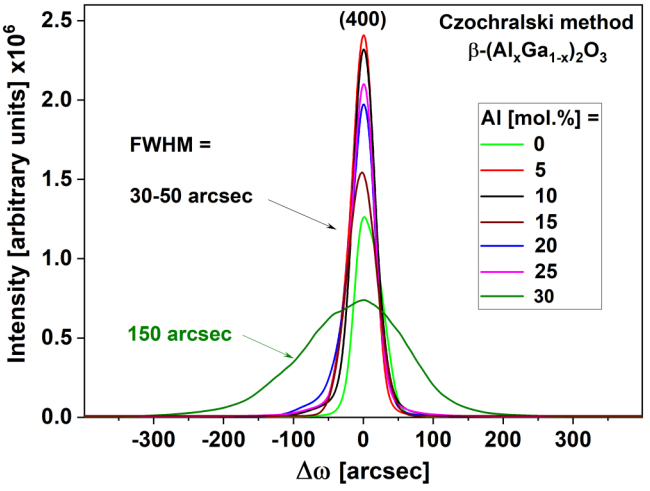

FIG. 4. X-ray rocking curves of crystal samples prepared from 20 mm diameter β-$(Al_xGa_{1-x})_2O_3$ single crystals grown by the Czochralski method with x = 0–0.30.

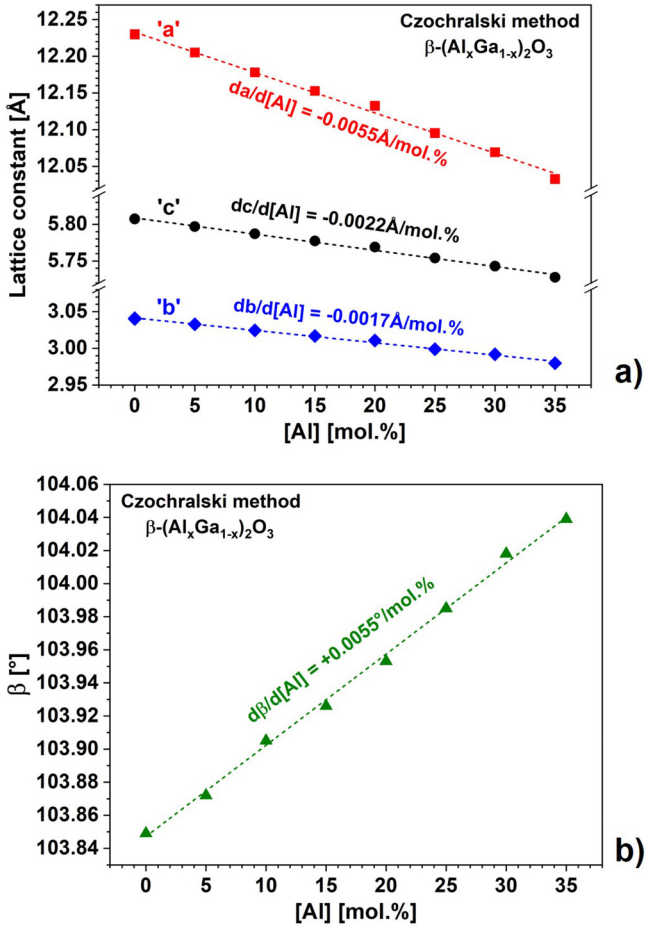

FIG. 5. (a) Lattice constants a, b, and c, and (b) β angle between [100] and [001] directions of the monoclinic β-$(Al_xGa_{1-x})_2O_3$ system vs [Al] (x = 0–0.35). For this purpose, the samples were selected from the bottom parts of crystals doped with [Al] = 0–30 mol. % in the melt and having a similar crystallization fraction of 25%–28%. For [Al] = 35 mol. % in the melt, a sample from a bottom part of a crystal co-doped with Si was used.

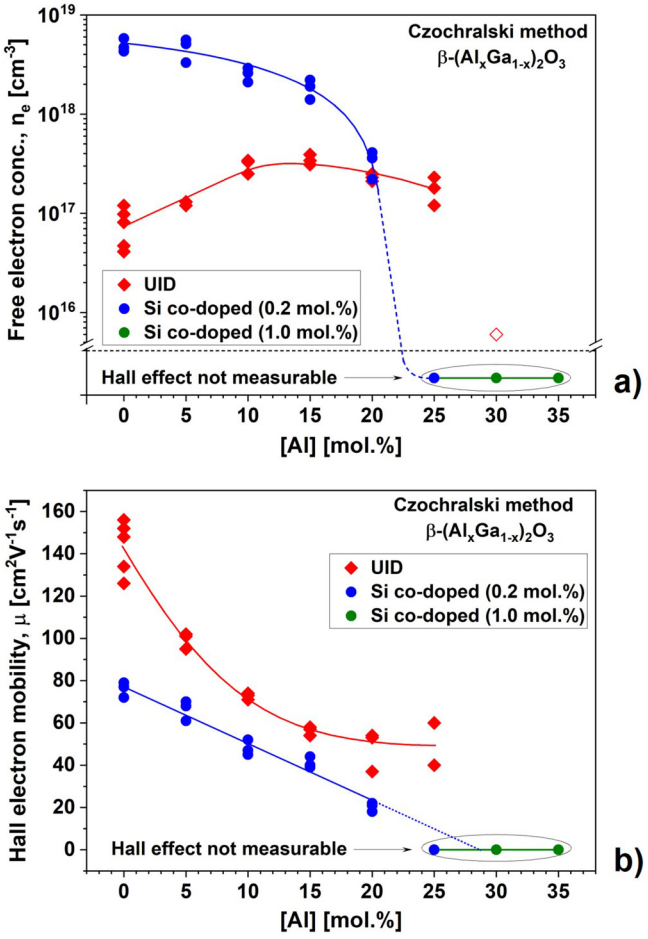

FIG. 6. Free electron concentration (a) and Hall electron mobility (b) of β-$(Al_xGa_{1-x})_2O_3$ (x = 0–0.35) crystals grown by the Czochralski method without intentional co-coping (red) and co-doped with Si (blue 0.2 mol. % and green 1 mol. %). The measurements were done on minimum three samples from each crystal (some points overlap with each other). The open red diamond in (a) is from the C–V measurement, as the Hall effect was difficult to measure. UID—unintentionally doped with free carriers.

in Fig. 2(a)]. At [Al] = 30 mol. %, it was difficult to measure the Hall effect, but the samples showed some electrical conductivity according to C–V measurements [open red diamond in Fig. 6(a)]. The origin of the conductivity arises mainly from residual Si (see Fig. 7) and hydrogen, as we discussed previously,[34] although the involvement of hydrogen in the electrical conductivity of β-$(Al_xGa_{1-x})_2O_3$ seems to be more complex according to the theoretical study of Mu *et al.*[47] In the case of crystals with no intentional Si doping, [Si] is at a level of just above 10^{17} cm^{-3}, similar to measured n_e values, although not the same. Hydrogen, that is present in Czochralski-grown β-Ga_2O_3 crystals,[34] may form either shallow donors or passivate compensating acceptors. A slight increase in the free electron concentration in UID crystals with [Al] = 0–15 mol. % that gives rise to more bluish coloration could, therefore, arise from a higher Si and/or H concentration, e.g., from the Al_2O_3 starting material, incidental contamination, and/or growth atmosphere.

β-$(Al_xGa_{1-x})_2O_3$ single crystals intentionally co-doped with [Si] = 0.2 mol. % in the melt [crystals in the second row in Fig. 2(a)] show a noticeable decrease in n_e values with [Al] from $4–6 \times 10^{18}$ cm^{-3} at [Al] = 0 mol. % to $2–4 \times 10^{17}$ cm^{-3} at [Al] = 20 mol. %. At higher [Al] = 25–35 mol. %, the Hall effect was not measurable (resistivity > 10^8 Ω cm), even at five times higher doping level in the melt (1 mol. %). Such behavior is not observed in crystals with no intentional co-doping. In Si-doped crystals, the primary source of the electrical conductivity is supposed to be Si substituting Ga in the crystal lattice and forming shallow donors. However, the β-$(Al_xGa_{1-x})_2O_3$ system with interacting various point defects is very complex to clearly conclude the electrical

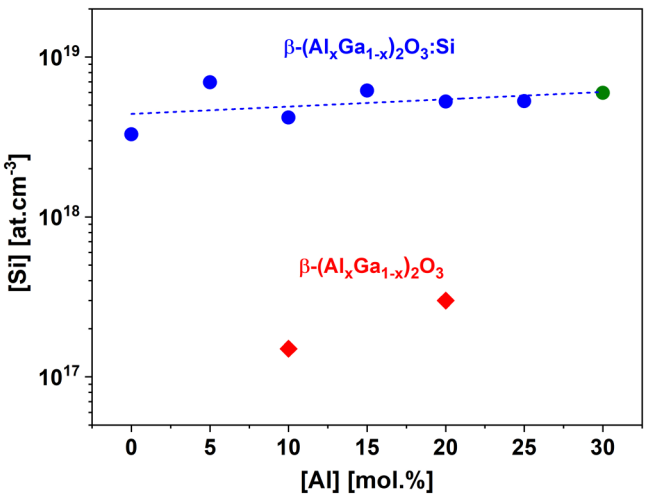

FIG. 7. Si (by SIMS) vs Al concentration in β-$(Al_xGa_{1-x})_2O_3$ single crystals grown by the Czochralski method.

response of Si co-doped to Al doping [Fig. 6(a)]. SIMS measurements of [Si] in the obtained crystals, as shown in Fig. 7, revealed high and almost constant [Si] between 3 and 7×10^{18} cm^{-3} for [Si] = 0.2 and 1 mol. % in the melt. Additionally, no difference in Si incorporation, regardless of the doping level in the melt being 0.2 or 1 mol. %, suggests an upper limit for substitutional Si incorporation as the competition between Ga and Si incorporation on the Ga lattice sites.[48]

According to theory, Si prefers to occupy tetrahedral sites $Ga_{(I)}$, while Al prefers to occupy octahedral sites $Ga_{(II)}$ in the β-Ga_2O_3 crystal lattice,[49,19] although Johnson *et al.*[28] state that Al may occupy both Ga sites in thin films. Also, as more $Ga_{(II)}$ sites are occupied by Al, more Ga tends to occupy $Ga_{(I)}$ sites, competing this way with Si. In these cases, a low effective segregation coefficient of Si in the Ga_2O_3 melt during growth by the Czochralski method and a high effective segregation coefficient of Al, k_{eff}(Si) = 0.1 and k_{eff}(Al) = 1.1, respectively,[33,44] would, indeed, decrease the substitutional incorporation of Si into the crystal lattice. However, [Si] in the crystals does not decrease with [Al], as shown in Fig. 7.

[Si] is only matched by n_e for low [Al] in co-doped crystals; hence, the higher the [Al], the lower the ratio n_e/[Si]. Additionally, we can conclude from the typical spiral shape of the crystals [see Fig. 2(a), row 2] that the crystals are highly electrically conducting at growth temperatures. Hence, we can exclude the segregation of silicon on electrically inactive sites since Si must be responsible for the high conductivity. One may also consider the shallow-to-deep level transition of Si with [Al], but theoretical works claim Si to be an effective shallow donor even up to [Al] = 70–85 mol. %.[19,47] This would require further experimental verification of the Si activation energy vs [Al]. However, this explanation is very unlikely since [Si] and n_e coincide in UID crystals with [Al] = 20 mol. % leading to the strongly supported assumption of silicon being a shallow donor, at least in crystals up to [Al] = 20 mol. %.

Likely, a fast decrease in n_e vs [Al] in Si co-doped crystals arises from the compensation of the electrical conductivity. Most occurring residual impurities forming acceptors in melt-grown crystals, i.e., Mg and Fe are at concentrations below 30 wt. ppm (measured by ICP-OES), which are not sufficient to compensate the electrical conductivity (this would had also been happened with UID crystals that have similar levels of residual [Mg] and [Fe]). However, other compensating mechanisms may dominate, in particular, those involving gallium vacancies V_{Ga} and hydrogen in a combination with Si. Although the oxygen concentration of 2 vol. % in the growth atmosphere may not be sufficient to form a high density of V_{Ga} in UID crystals, Si co-doping promotes the formation of V_{Ga}.[50] On the other hand, hydrogen passivates V_{Ga}. Taking into account the measured high [Si] = $3–7 \times 10^{18}$ cm^{-3}, [H] < 2×10^{18} cm^{-3},[34] and unknown [V_{Ga}] in Si co-doped crystals, it is not obvious at this moment whether this compensating mechanism dominates. Although $(Si_{Ga(I)}–H_I)^0$ complexes are theoretically considered compensating acceptors in thin films,[47] they are unstable at high temperatures and would not form during crystal growth. Annealing Si co-doped samples with [Al] = 15–30 mol. % in air at 800 and 1100 °C for 15h (to dissociate the complexes) did not increase the electrical conductivity at all (i.e., Si was not activated).

One may consider other dopants forming shallow donors in β-$(Al_xGa_{1-x})_2O_3$, such as those theoretically discussed by Varley (C, Ge, Sn, Hf, Zr, and Ta),[19] but even theoretically, they seem not to be as effective as Si and are not detectable in the grown crystals. In the case of Sn doping, often used for doping β-Ga_2O_3, two issues should be considered: (i) the same site occupancy as Al that would lead, indeed, to the competition and (ii) very high vapor pressure of SnO (0.02 bar at 1900 °C), which leads to high, continuous losses of Sn through evaporation as the growth proceeds (non-uniform Sn distribution in the crystals), even at high initial doping level in the melt (> 1 mol. %).[34] Ge cannot be used as a dopant due to very high partial pressure of GeO, leading to entire losses of Ge during growth from the melt.[34]

Both 20 and 55 mm diameter crystals co-doped with Mg, as shown in Fig. 2(a) (third row) and Fig. 2(b), revealed an electrically insulating or semi-insulation state (resistivity > 10^8 Ω cm). This means that [Mg] = 0.3–0.5 mol. % in the melt efficiently compensates the electrical conductivity over the entire range of [Al] = 0–25 mol. %.

Hall electron mobility, μ, for the same β-$(Al_xGa_{1-x})_2O_3$ single crystal samples are shown in Fig. 6(b). Here, the μ values gradually decrease for crystal samples with no co-dopants from 125–156 cm^2 V^{-1} s^{-1} at [Al] = 0 mol. % to 40–60 cm^2 V^{-1} s^{-1} at [Al] = 25 mol. %. At [Al] ≥ 20 mol. %, the electron mobility seems to saturate. This is in line with our previous study[35,36] showing a small decrease in the electron mobility in Czochralski-grown β-Ga_2O_3 single crystals doped with [Al] = 5 mol. %. As the n_e values are low or moderate, the drop of the electron mobility arises mainly from lattice distortion (minor impact of scattering at ionized impurities) that increases with [Al]. In other words, lattice distortion increases scattering at phonons. For more accurate analysis of the electron mobility profile, it is necessary to include a small increase in the effective electron mass and a decrease in the static dielectric constant with [Al].[20] Finally, an increased alloy scattering

contributes to the reduction in mobility with increasing [Al]. A similar situation is observed in the case of samples co-doped with Si; however, absolute μ values are smaller due to additional scattering at ionized impurities, while the mobility profile is substantially linear. The electron mobility decreases from 72–80 $cm^2 V^{-1} s^{-1}$ at [Al] = 0 mol. % to 18–21 $cm^2 V^{-1} s^{-1}$ at [Al] = 20 mol. %. At [Al] ≥ 25 mol. %, the crystals became electrically insulating, even at five times higher [Si] in the melt (1 mol. %). Nonetheless, the extrapolation of the electron mobility to higher [Al] values indicates a drop of the mobility to virtually zero already at [Al] = 29 mol. % in the melt. At the moment, these findings suggest a limitation of highly conducting β-$(Al_xGa_{1-x})_2O_3$ substrates for power devices in the vertical configuration. To keep $n_e > 10^{18}$ cm^{-3} in such substrates, [Al] in the crystals should not be higher than 15–20 mol. %. For comparison, MOCVD-grown, Si co-doped heteroepitaxial β-$(Al_xGa_{1-x})_2O_3$ films reported by Alema *et al.*[27] had mobility values of 10–35 $cm^2 V^{-1} s^{-1}$ for [Al] = 12–24 mol. % and free electron concentration of ~10^{19}–10^{20} cm^{-3}, which decreased with [Al].

D. Optical properties

The near-edge absorption of β-$(Al_xGa_{1-x})_2O_3$ single crystals was gathered by optical absorbance measurements, as shown in Fig. 8(a). (100)-oriented samples enabled to probe the absorption coefficient with the polarization vector parallel to the [010] and [001] directions. The absorption edge with E||b-axis shifts with [Al] from about 270 nm at [Al] = 0 mol. % to about 230 nm at [Al] = 30 mol. %. A similar shift of the absorption edge toward shorter wavelengths is also observed for the E||c-axis. So, the absorption edge of β-$(Al_xGa_{1-x})_2O_3$ is entirely confined to the UV-C spectral region, close to VUV, suitable for deep UV optoelectronic applications, such as photodetectors or optical filters.

As the samples were prepared from bottom parts of UID crystals of similar crystallization fraction with moderate and similar values of $n_e \lesssim 3 \times 10^{17}$ cm^{-3}, an impact of the free carriers on the near-edge absorption and, thus, on the bandgap (known as Burstein–Moss shift), is neglectable small. The Burstein–Moss shift occurs in degenerately semiconducting β-Ga_2O_3 with $n_e > 3 \times 10^{18}$ cm^{-3}.[36] Indeed, this was noticed by Shimamura *et al.*[51] in degenerately semiconducting β-Ga_2O_3 crystals, where $n_e = 7 \times 10^{18}$ cm^{-3} in the crystals, which led to near-edge absorption shift but by about 2 nm only. The Burstein–Moss shift that occurs in degenerately semiconducting β-Ga_2O_3 has been theoretically shown by Zheng *et al.*[52]

Bandgap values, E_g, were evaluated from the near-edge absorption coefficients for direct transitions [$\alpha \propto (E-E_g)^{1/2}$] and are shown in Fig. 8(b) for E||b and E||c. The E_g values increase substantially linearly and equally for both polarizations, by 0.75 eV at [Al] = 30 mol. % with respect to pure β-Ga_2O_3. The increase rate of the E_g for these experimental results is about 25 meV/mol. %. Because the measured β-$(Al_xGa_{1-x})_2O_3$ single crystal samples had n_e values far below the values of degenerately semiconducting crystals, the observed bandgap increase arises substantially from Al doping only.

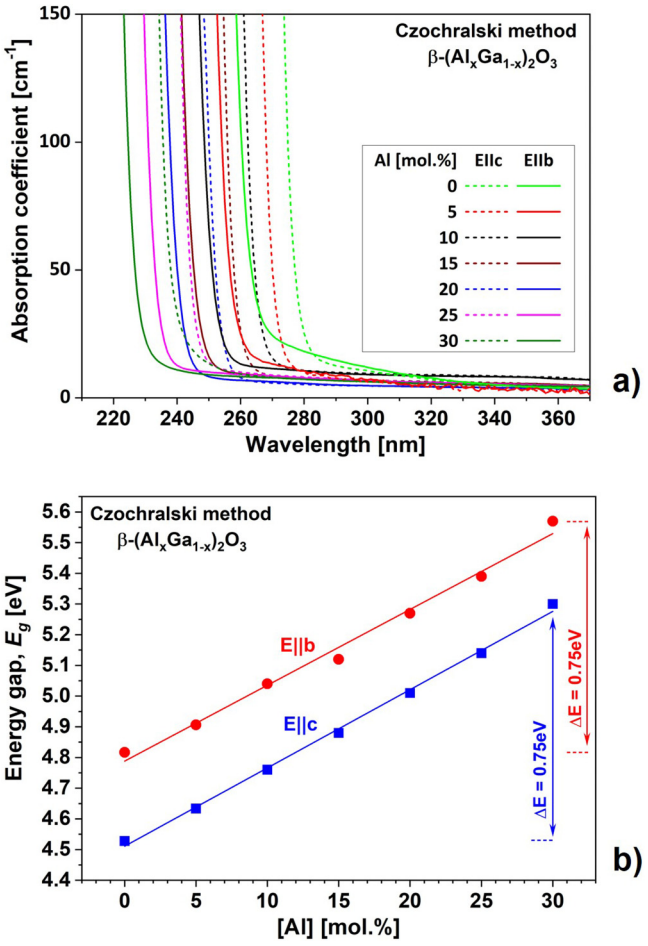

FIG. 8. Near-edge absorption coefficient (a) from absorbance measurements and direct bandgap for polarization parallel to b- and c-axes (b) of β-$(Al_xGa_{1-x})_2O_3$ single crystals grown by the Czochralski method.

E. Baliga figure of merit

Having μ and E_g values measured for a wide [Al] range in β-$(Al_xGa_{1-x})_2O_3$ single crystals, it becomes possible to estimate the experimental values of Baliga figure of merit (BFOM), which is a measure of conduction losses in FETs.[53] The BFOM for different device configurations is defined by Bajaj *et al.*[54] as follows:

$$\text{BFOM} = \varepsilon \times \mu \times E_c^3 \text{ for devices in the vertical configuration,} \quad (1)$$

$$\text{BFOM} = \varepsilon \times \mu \times E_c^2 \text{ for devices in the lateral configuration,} \quad (2)$$

where ε, μ, and E_c are the static dielectric constant, electron mobility, and critical breakdown field, respectively. E_c for materials with

a direct bandgap (β-Ga_2O_3 can be considered a quasi-direct bandgap material due to tiny differences between direct and indirect transitions of 50 meV)[1] is given by Hudgins *et al.* as follows:[55]

$$E_c\ (\text{direct bandgap}) = 1.73 \times 10^5 \times E_g^{2.5}, \quad (3)$$

$$E_c\ (\text{indirect bandgap}) = 2.38 \times 10^5 \times E_g^{2}. \quad (4)$$

Substituting Eq. (3) into Eqs. (1) and (2) and using $\varepsilon = 10.53$ for a direction perpendicular to [010][56] and μ values for β-$(Al_xGa_{1-x})_2O_3$ single crystals with no intentional co-dopants [crystals in Fig. 2(a), first row] and Si-doped [crystals in Fig. 2(a), second row], one can obtain the estimated values of BFOMs for devices in both lateral and vertical configurations, as depicted in Fig. 9(a). For low and moderate n_e values of 0.4–3 × 10^{17} cm^{-3} (no intentional co-dopants), the μ decrease is greater than the gain of the bandgap, resulting in a decrease in BFOM with [Al] ≤ 15 mol. %. However, for [Al] > 15 mol. %, μ seems to saturate, and the bandgap gain dominates, which leads to an increase in BFOM, but the absolute BFOM value for [Al] = 25 mol. % is still lower than that of pure β-Ga_2O_3. Taking into account the fact that typical μ values of homoepitaxial films are not higher than those of single crystals at similar n_e values, while the bandgap is the intrinsic material property, BFOM values of homoepitaxial β-$(Al_xGa_{1-x})_2O_3$ films are expected to be similar. Somewhat higher μ and, thus, BFOMs can be gained in homoepitaxial thin films with yet lower n_e values (10^{15}–10^{16} cm^{-3}), which is rather not achievable for bulk crystals without compensation control.

When considering Si co-doped samples (n_e = 0.4–5 × 10^{18} cm^{-3}), the BFOM gradually decreases with [Al] = 0–15 mol. %. For [Al] > 15 mol. %, the BFOM decreases faster, in contrast to crystals with no intentional doping. Here, a substantially linear decrease in the electron mobility and its lower values over the whole [Al] range overcome the bandgap enlargement. The behavior of the BFOM for electronic devices in both lateral and vertical configurations is very similar.

Figure 9(b) shows the BFOMs of β-$(Al_xGa_{1-x})_2O_3$ single crystals scaled to BFOM of silicon, where the following Si properties were used:[55] indirect E_g = 1.12 eV, μ = 1400 $cm^2\,V^{-1}\,s^{-1}$, and ε = 11.9. For vertical devices, there is a gain of BFOMs with respect to Si by 3250 and 1600 for pure β-Ga_2O_3 having moderate and high n_e values, respectively, in line with values of 2000–3400 shown by Higashiwaki *et al.*,[57] while for lateral devices, there is a gain of BFOMs with respect to Si by 100 and 50, respectively. The BFOM gain is strongly affected by [Al] in the case of vertical devices compared to lateral devices.

The experimental BFOM vs [Al] in β-$(Al_xGa_{1-x})_2O_3$ single crystals are very similar to some of the BFOMs theoretically predicted by Varley,[20] who calculated BFOMs for different electron mobility profiles vs [Al] (Fig. 7 in Ref. 20). The present study, made on the bulk single crystals of high structural quality, provides detailed experimental profiles vs [Al] that can narrow theoretical studies.

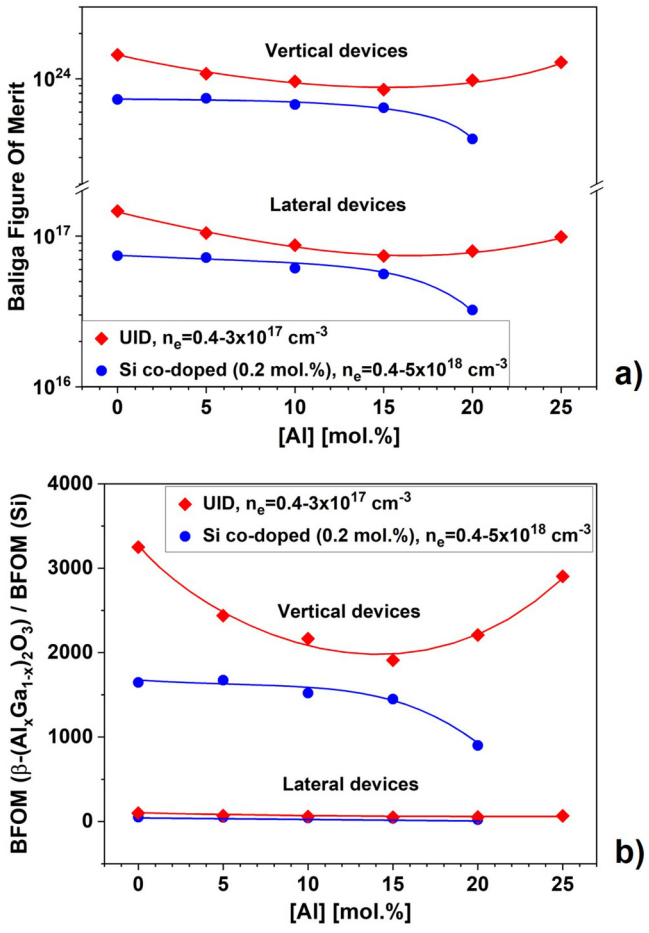

FIG. 9. Experimental Baliga figure of merit (BFOM) of Czochralski-grown β-$(Al_xGa_{1-x})_2O_3$ (x = 0–0.25) single crystals for field-effect transistors in lateral and vertical configurations: (a) absolute values and (b) scaled to Si values. For calculations, the highest measured electron mobilities were used, and the corresponding free electron concentration (n_e) ranges are shown in the figure legend.

IV. CONCLUSIONS

The present study demonstrates the capability of growing bulk β-$(Al_xGa_{1-x})_2O_3$ single crystals of 20 and 55 mm diameter by the Czochralski method with [Al] up to 30 mol. % in the melt ([Al] = 33–36 mol. % in the crystals). The crystals are of high structural quality and maintain a single-crystalline, monoclinic structure. Higher [Al] in the melt resulted mostly in polycrystal formation. In addition to Al, the crystals were also co-doped with Si and Mg. The growth challenges arise from a large separation between liquidus and solidus of the Ga_2O_3–Al_2O_3 solid-solution system, as well as from the lattice distortion. It is important to use the crystal seeds of a similar composition to the melt composition.

The bandgap increases by 0.75 eV for [Al] = 30 mol. % in the melt in reference to pure β-Ga_2O_3, equally for polarizations parallel to both b- and c-axes. The bulk β-$(Al_xGa_{1-x})_2O_3$ crystals with no intentional co-doping are n-type semiconductors over the whole doping range [Al] = 0–25 mol. % (n_e = 0.4–4 × 10^{17} cm^{-3}), while Si co-doped crystals show a drastic drop of the free electron

concentration (from $n_e = 4–6 \times 10^{18}$ cm^{-3} at [Al] = 0 mol. %) to $n_e = 2–4 \times 10^{17}$ cm^{-3} at [Al] = 20 mol. %), in particular, at [Al] > 15 mol. % and became electrically insulating at [Al] ≥ 25 mol. %, even at high Si doping level (1 mol. %). The corresponding electron mobility with no intentional co-dopants decreases from 125–156 cm^2 V^{-1} s^{-1} at [Al] = 0 mol. % to 40–60 cm^2 V^{-1} s^{-1} at [Al] = 25 mol. % with saturation signs at [Al] ≥ 20 mol. %, which indicates extra scattering caused mainly by lattice distortion. On the other hand, the electron mobility of Si co-doped crystals decreases linearly from 70–80 cm^2 V^{-1} s^{-1} at [Al] = 0 mol. % to 18–22 cm^2 V^{-1} s^{-1} at [Al] = 20 mol. %, as the result of additional scattering at ionized impurities.

Measured energy gaps and electron mobilities enabled us to calculate the Baliga figures of merit (BFOMs), which are similar in shape for power devices in both lateral and vertical configurations. Over the whole [Al] range, the highest BFOM values for bulk β-$(Al_xGa_{1-x})_2O_3$ crystals were obtained [Al] = 0 mol. % (pure β-Ga_2O_3), whether co-doped with Si or not, as the mobility drop is not sufficiently compensated by the bandgap increase. All crystals co-doped with Mg were electrical insulators.

ACKNOWLEDGMENTS

This work was funded by the Deutsche Forschungsgemeinschaft (DFG) project under Grant Nos. GA 2057/5-1 and PO 2659/3-1. It was partly performed in the framework of GraFOx, a Leibniz-Science Campus, partially funded by the Leibniz Association—Germany, and partially funded by the BMBF under Grant No. 16ES1084K. The work by A.F. was partially funded by Leibniz-Gemeinschaft (Senatsausschuss Wettbewerb) under Project No. K429/2021. The authors express their gratitude to Thomas Wurche from Leibniz-Institut für Kristallzüchtung (IKZ) for cutting single crystals and to Michael Schulze from IKZ for critical reading of the paper.

AUTHOR DECLARATIONS

Conflict of Interest

The authors have no conflicts to disclose.

Author Contributions

Zbigniew Galazka: Conceptualization (lead); Data curation (equal); Formal analysis (lead); Funding acquisition (equal); Investigation (lead); Project administration (lead); Resources (equal); Supervision (lead); Validation (equal); Visualization (equal); Writing – original draft (lead); Writing – review & editing (lead). **Andreas Fiedler:** Data curation (equal); Formal analysis (equal); Methodology (equal); Validation (equal); Visualization (equal); Writing – review & editing (equal). **Andreas Popp:** Conceptualization (supporting); Funding acquisition (equal); Project administration (supporting); Supervision (supporting); Writing – review & editing (equal). **Steffen Ganschow:** Conceptualization (supporting); Writing – review & editing (equal). **Albert Kwasniewski:** Data curation (equal); Formal analysis (equal); Methodology (equal); Visualization (equal); Writing – review & editing (equal). **Palvan Seyidov:** Data curation (equal); Formal analysis (equal); Methodology (equal); Visualization (equal); Writing – review & editing (equal). **Mike Pietsch:** Data curation (equal); Methodology (equal); Writing – review & editing (equal). **Andrea Dittmar:** Data curation (equal); Methodology (equal); Writing – review & editing (equal). **Saud Bin Anooz:** Conceptualization (supporting); Data curation (equal); Methodology (equal); Visualization (equal); Writing – review & editing (equal). **Klaus Irmscher:** Conceptualization (supporting); Methodology (equal); Writing – review & editing (equal). **Manuela Suendermann:** Resources (equal); Writing – review & editing (equal). **Detlef Klimm:** Conceptualization (supporting); Writing – review & editing (equal). **Ta-Shun Chou:** Conceptualization (supporting); Writing – review & editing (equal). **Jana Rehm:** Conceptualization (supporting); Writing – review & editing (equal). **Thomas Schroeder:** Conceptualization (supporting); Writing – review & editing (equal). **Matthias Bickermann:** Conceptualization (supporting); Writing – review & editing (equal).

DATA AVAILABILITY

The data that support the findings of this study are available within the article.

REFERENCES

[1]C. Janowitz, V. Scherer, M. Mohamed, A. Krapf, H. Dwelk, R. Manzke, Z. Galazka, R. Uecker, K. Irmscher, R. Fornari, M. Michling, D. Schmeißer, J. R. Weber, J. B. Varley, and C. G. Van de Walle, New J. Phys. **13**, 085014 (2011).
[2]M. Higashiwaki, K. Sasaki, A. Kuramata, T. Masui, and S. Yamakoshi, Appl. Phys. Lett. **100**, 013504 (2012).
[3]M. Higashiwaki, K. Sasaki, H. Murakami, Y. Kumagai, A. Koukitu, A. Kuramata, T. Masui, and S. Yamakoshi, Semicond. Sci. Technol. **31**, 034001 (2016).
[4]S. I. Stepanov, V. I. Nikolaev, V. E. Bougrov, and A. E. Romanov, Rev. Adv. Mater. Sci. **44**, 63–86 (2016).
[5]M. A. Mastro, A. Kuramata, J. Calkins, J. Kim, F. Ren, and S. J. Pearton, ECS J. Solid State Sci. Technol. **6**, P356–P359 (2017).
[6]Z. Galazka, Semicond. Sci. Technol. **33**, 113001 (2018).
[7]M. Baldini, Z. Galazka, and G. Wagner, Mater. Sci. Semicond. Proc. **78**, 132–146 (2018).
[8]S. J. Pearton, J. Yang, P. H. Cary IV, F. Ren, J. Kim, M. J. Tadjer, and M. A. Mastro, Appl. Phys. Rev. **5**, 011301 (2018).
[9]M. Razeghi, J. H. Park, R. McClintock, D. Pavlidis, F. H. Teherani, D. J. Rogers, B. A. Magill, G. A. Khodaparast, Y. Xu, J. Wu, Vinayak, and P. Dravid, Proc. SPIE **10533**, 105330R1–105330R23 (2018).
[10]M. J. Tadjer, J. L. Lyons, N. Nepal, J. A. Freitas, Jr., A. D. Koehler, and G. M. Foster, ECS J. Solid State Sci. Technol. **8**, Q3187–Q3194 (2019).
[11]J. Zhang, J. Shi, D.-C. Qi, L. Chen, and K. H. L. Zhang, APL Mater. **8**, 020906 (2020).
[12]R. Singh, T. R. Lenka, D. K. Panda, R. T. Velpula, B. Jain, H. Q. T. Bui, and H. P. T. Nguyen, Mater. Sci. Semicond. Process. **119**, 105216 (2020).
[13]M. H. Wong and M. Higashiwaki, IEEE Trans. Electron. Devices **67**, 3925–3937 (2020).
[14]C. Wang, J. Zhang, S. Xu, C. Zhang, Q. Feng, Y. Zhang, J. Ning, S. Zhao, H. Zhou, and Y. Hao, J. Phys. D: Appl. Phys. **54**, 243001 (2021).
[15]*Gallium Oxide: Technology, Devices and Applications*, edited by S. Pearton, F. Ren, and M. Mastro (Elsevier, 2018).
[16]*Gallium Oxide: Crystal Growth, Materials Properties, and Devices*, edited by M. Higashiwaki and S. Fujita (Springer Nature, 2020).
[17]Z. Galazka, *Transparent Semiconducting Oxides—Bulk Crystal Growth and Fundamental Properties* (Jenny Stanford Publishing, 2020).

[18]H. Peelaers, J. B. Varley, J. S. Speck, and C. G. Van de Walle, Appl. Phys. Lett. **112**, 242101 (2018).
[19]J. B. Varley, A. Perron, V. Lordi, D. Wickramaratne, and J. L. Lyons, Appl. Phys. Lett. **116**, 172104 (2020).
[20]J. B. Varley, J. Mater. Res. **36**, 4790–4803 (2021).
[21]S. Mu, M. Wang, H. Peelaers, and C. G. Van de Walle, APL Mater. **8**, 091105 (2020).
[22]S. W. Kaun, F. Wu, and J. S. Speck, J. Vac. Sci. Technol. A **33**, 041508 (2015).
[23]A. F. M. A. U. Bhuiyan, Z. Feng, J. M. Johnson, H.-L. Huang, J. Sarker, M. Zhu, M. R. Karim, B. Mazumder, J. Hwang, and H. Zhao, APL Mater. **8**, 031104 (2020).
[24]A. F. M. A. U. Bhuiyan, Z. Feng, J. M. Johnson, H.-L. Huang, J. Hwang, and H. Zhao, Appl. Phys. Lett. **117**, 252105 (2020).
[25]A. F. M. A. U. Bhuiyan, Z. Feng, J. M. Johnson, H.-L. Huang, J. Hwang, and H. Zhao, Cryst. Growth Des. **20**, 6722–6730 (2020).
[26]A. F. M. A. U. Bhuiyan, Z. Feng, L. Meng, and H. Zhao, J. Mater. Res. **36**, 4804–4815 (2021).
[27]F. Alema, T. Itoh, S. Vogt, J. S. Speck, and A. Osinsky, Jpn. J. Appl. Phys. **61**, 100903 (2022).
[28]J. M. Johnson, H.-L. Huang, M. Wang, S. Mu, J. B. Varley, A. F. M. A. U. Bhuiyan, Z. Feng, N. K. Kalarickal, S. Rajan, H. Zhao, C. G. Van de Walle, and J. Hwang, APL Mater. **9**, 051103 (2021).
[29]A. F. M. A. U. Bhuiyan, Z. Feng, J. M. Johnson, Z. Chen, H.-L. Huang, J. Hwang, and H. Zhao, Appl. Phys. Lett. **115**, 120602 (2019).
[30]A. Fiedler, R. Schewski, M. Baldini, Z. Galazka, G. Wagner, M. Albrecht, and K. Irmscher, J. Appl. Phys. **122**, 165701 (2017).
[31]R. Schewski, M. Baldini, K. Irmscher, A. Fiedler, T. Markurt, B. Neuschulz, T. Remmele, T. Schulz, G. Wagner, Z. Galazka, and M. Albrecht, J. Appl. Phys. **120**, 225308 (2016).
[32]S. Bin Anooz, R. Grüneberg, C. Wouters, R. Schewski, M. Albrecht, A. Fiedler, K. Irmscher, Z. Galazka, W. Miller, G. Wagner, J. Schwarzkopf, and A. Popp, Appl. Phys. Lett. **116**, 182106 (2020).
[33]Z. Galazka, S. Ganschow, A. Fiedler, R. Bertram, D. Klimm, K. Irmscher, R. Schewski, M. Pietsch, M. Albrecht, and M. Bickermann, J. Cryst. Growth **486**, 82–90 (2018).
[34]Z. Galazka, K. Irmscher, R. Schewski, I. M. Hanke, M. Pietsch, S. Ganschow, D. Klimm, A. Dittmar, A. Fiedler, T. Schroeder, and M. Bickermann, J. Cryst. Growth **529**, 125297 (2020).
[35]Z. Galazka, R. Schewski, K. Irmscher, W. Drozdowski, M. E. Witkowski, M. Makowski, A. J. Wojtowicz, I. M. Hanke, M. Pietsch, T. Schulz, D. Klimm, S. Ganschow, A. Dittmar, A. Fiedler, T. Schroeder, and M. Bickermann, J. Alloys Compd. **818**, 152842 (2020).
[36]Z. Galazka, S. Ganschow, P. Seyidov, K. Irmscher, M. Pietsch, T.-S. Chou, S. Bin Anooz, R. Grueneberg, A. Popp, A. Dittmar, A. Kwasniewski, M. Suendermann, D. Klimm, T. Straubinger, T. Schroeder, and M. Bickermann, Appl. Phys. Lett. **120**, 152101 (2022).
[37]D. A. Bauman, D. I. Panov, D. A. Zakgeim, V. A. Spiridonov, A. V. Kremleva, A. A. Petrenko, P. N. Brunkov, N. D. Prasolov, A. V. Nashchekin, A. M. Smirnov, M. A. Odnoblyudov, V. E. Bougrov, and A. E. Romanov, Phys. Status Solidi A **218**, 2100335 (2021).
[38]J. Jesenovec, B. Dutton, N. Stone-Weiss, A. Chmielewski, M. Saleh, C. Peterson, N. Alem, S. Krishnamoorthy, and J. S. McCloy, J. Appl. Phys. **131**, 155702 (2022).
[39]I. Bhaumik, M. Soharab, R. Bhatt, A. Saxena, S. Sah, and A. K. Karnal, Opt. Mater. **109**, 110351 (2020).
[40]Z. Galazka, S. Ganschow, M. Bickermann, T. Schroeder, PCT/EP2022/078252, 2022.
[41]Z. Galazka, K. Irmscher, R. Uecker, R. Bertram, M. Pietsch, A. Kwasniewski, M. Naumann, T. Schulz, R. Schewski, D. Klimm, and M. Bickermann, J. Cryst. Growth **404**, 184–191 (2014).
[42]Z. Galazka, R. Uecker, D. Klimm, K. Irmscher, M. Naumann, M. Pietsch, A. Kwasniewski, R. Bertram, S. Ganschow, and M. Bickermann, ECS J. Solid State Sci. Technol. **6**, Q3007–Q3011 (2017).
[43]Z. Galazka, "Czochralski method," in *Gallium Oxide: Crystal Growth, Materials Properties, and Devices*, edited by M. Higashiwaki and S. Fujita (Springer Nature, 2020), pp. 15–36.
[44]Z. Galazka, J. Appl. Phys. **131**, 031103 (2022).
[45]Z. Galazka, R. Uecker, D. Klimm, and M. Bickermann, EP 3242965 B1, 2019.
[46]M. Mizuno, T. Yamada, T. Noguchi J. Ceram. Soc. Jpn. **83**, 175–177 (1975).
[47]S. Mu, M. Wang, J. B. Varley, J. L. Lyons, D. Wickramaratne, and C. G. Van deWalle, Phys. Rev. B **105**, 155201 (2022).
[48]T.-S. Chou, S. Bin Anooz, R. Grüneberg, N. Dropka, J. Rehm, T. T. V. Tran, K. Irmscher, P. Seyidov, W. Miller, Z. Galazka, M. Albrecht, and A. Popp, Appl. Phys. Lett. **121**, 032103 (2022).
[49]M. Wang, S. Mu, and C. G. Van de Walle, J. Appl. Phys. **130**, 185703 (2021).
[50]J. Uhlendorf, Z. Galazka, and H. Schmidt, Appl. Phys. Lett. **119**, 242106 (2021).
[51]K. Shimamura, E. G. Víllora, T. Ujiie, and K. Aoki, Appl. Phys. Lett. **92**, 201914 (2008).
[52]T. Zheng, Q. Wang, J.-N. Dang, W. He, L.-Y. Wang, and S.-W. Zheng, Comput. Mater. Sci. **174**, 109505 (2020).
[53]B. J. Baliga, IEEE Electron Device Lett. **10**, 455–457 (1989).
[54]S. Bajaj, T.-H. Hung, F. Akyol, D. Nath, and S. Rajan, Appl. Phys. Lett. **105**, 263503 (2014).
[55]J. L. Hudgins, G. S. Simin, E. Santi, and M. A. Khan, IEEE Trans. Power Electron. **18**, 907–914 (2003).
[56]A. Fiedler, R. Schewski, Z. Galazka, and K. Irmscher, ECS J. Solid State Sci. Technol. **8**, Q3083–Q3085 (2019).
[57]M. Higashiwaki, H. Murakami, Y. Kumagai, and A. Kuramata, Jpn. J. Appl. Phys. **55**, 1202A1 (2016).